An infrared eccentric photo-optometer

Austin Roorda [a,b,*], William R. Bobier [a], Melanie C.W. Campbell [a,b]

[a] *School of Optometry, University of Waterloo, Waterloo, Ontario, Canada N2L 3G1*
[b] *Guelph-Waterloo program for Graduate Work in Physics, University of Waterloo, Waterloo, Ontario, Canada N2L 3G1*

Abstract

An objective infrared optometer has been designed, based on the optical principles of eccentric photorefraction. A CCD camera with an eccentric infrared light source images the subject's pupil through a Badal optometer. The slope of the light distribution across the pupil is continuously recorded. Accommodative state is measured by moving the camera behind the Badal lens until the slope is zero. This position corresponds to the case where the camera is conjugate with the retina of the observer. In this Badal optometer, the irradiance of light at the pupil plane, the sensitivity of the photorefractor, and the focal setting of the camera lens remain constant for all positions of the camera from the eye. The repeatability of a single measure of refractive state in a cycloplegic eye was less than 0.05 D. Static accommodative responses taken from 3 subjects in both closed and open loop conditions provided expected stimulus/response measures. The instrument can also be adapted to measure dynamic accommodation. © 1998 Elsevier Science Ltd. All rights reserved.

1. Introduction

Through the application of the optical principles of eccentric photorefraction and the incorporation of a Badal optometer, a new objective infrared optometer has been developed suitable for rapid measures of static accommodation. The instrument locates the plane in physical space that is conjugate with the retina by physically moving an eccentric photorefractor behind a Badal optometer lens. This nulling principle is analogous to subjective methods such as stigmoscopy [1] and laser speckle refraction [2,3]. The eccentric photo-optometer, however, is objective, allowing the nulling decisions to be made by the experimenter or through computer control. The design of the instrument has some similarities to the Humphrey atotrefractor which uses a Foucault knife edge instrument with a Badal optometer to measure refractive state. The instrument shares the same advantages as most objective optometers [4–6]. First, the objective measure reduces the demands and level of experience required of the

subject. Second, infrared light is used, which does not distract the subject.

In eccentric photorefraction, the refractive state of the eye is determined based on the appearance of the light distribution, or reflex, that appears in the pupil from a double passage of light through the optical system. From the earliest developments, eccentric photorefraction instruments have always required an experimental calibration [7–9]. In spite of the theoretical derivation of crescent extent as a function of refractive state [8,10], actual measurements have been hampered by thresholding and aberrations of the eye. The calibration of an eccentric photorefractor entailed a controlled study to find how the reflex slope (or crescent extent) changed in response to controlled defocus of a human or artificial eye. The result of the calibration was a look-up table or calibration curve from which estimations of the refractive state could be inferred based on the appearance of the reflex. The calibration curves represent averaged data where considerable spread was found between individuals [11]. This diversity is attributed to variability in monochromatic aberrations between individuals, differences in retinal reflectivity and differences in pupil size. In the instrument described here, the photorefraction reflex is neutralized

---

* Corresponding author. Present address: Center for Visual Science, University of Rochester, Rochester, NY 14627, USA. E-mail: aroorda@cvs.rochester.edu
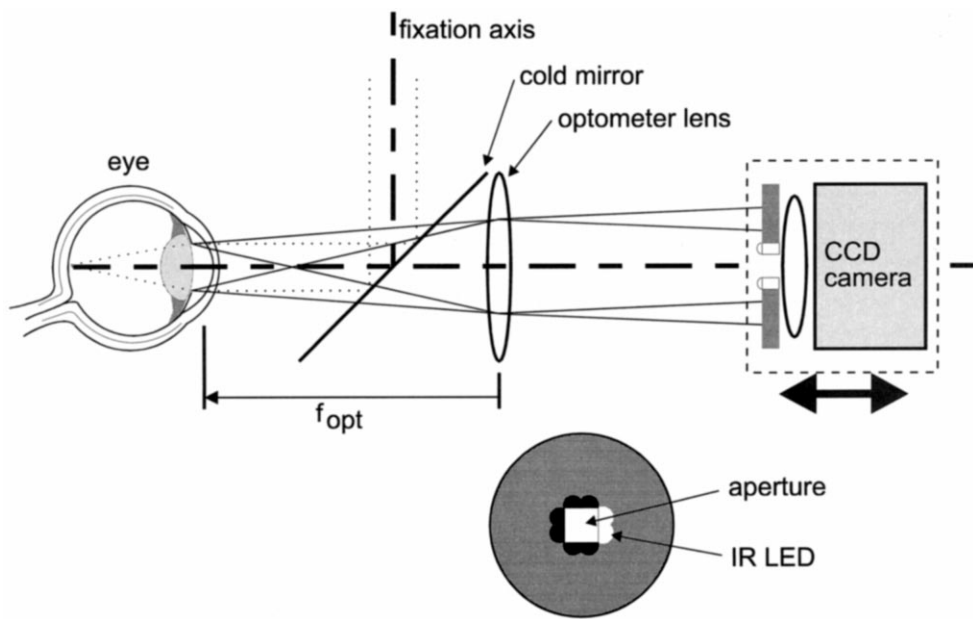
Fig. 1. The Eccentric Photo-optometer. The subject is aligned with the optometer axis through the use of a bite bar or chin rest. Alignment is controlled using an $x-y-z$ translation stage while monitoring the pupil position. The subject views the stimulus to accommodation along the fixation axis after reflection from the cold-mirror. The photorefractor (aperture, light source, lens and CCD camera) is placed on a track (not shown) and slides freely along the axis behind the optometer lens. The camera is focused on the subject's pupil and video output is sent to a computer with a frame grabbing board. A front view of the aperture and light source is shown in the lower figure. The eccentric photorefractor uses four pairs of LEDs, one pair on each side of the 8 mm aperture. Only one pair is operated at a time as is shown in the figure. For measurements along the horizontal meridian or vertical meridian one of the horizontally or vertically eccentric pairs are used, respectively (filled circles). The aperture and LED assembly fits onto the standard 50 mm camera lens that is connected to the CCD camera.

(flat slope) by moving the camera, thereby making calibration unnecessary. Neutralization occurs when the subject's retina is conjugate with the photorefractor and is not dependent on the camera type or light source configuration (provided that a small eccentricity is used). For photorefractor positions outside of this region, the slope of the pupil reflex increases with refractive error [12,9]. It has been shown that monochromatic aberrations also affect the shape of the photorefractive profile [13]. In the eccentric photo-optometer, effects of aberrations are minimized by using a slope-based instrument and by using a 5 mm artificial pupil at the subject's eye. A more efficient calibration procedure is also described that should allow the instrument to measure dynamic accommodation in this system at 10 Hz.

The feasibility of using an eccentric photorefraction device to measure dynamic accommodation has been demonstrated by Schaeffel et al. [9]. Their instrument used the infrared photoretinoscope to dynamically measure changes in accommodation at 5.3 Hz with a precision of 0.2–0.4 D [14]. An advantage of their video-based instrument was the ability to simultaneously measure pupil size and gaze direction. Their instrument, however, did not utilise the advantages of the Badal optometer (see section 2.2) and it required careful calibration since it was not based on the neutralisation of the reflex.

2. Eccentric photo-optometer design and operation

2.1. Photorefractor

The eccentric photorefractor design uses a small square aperture (8 mm sides) with a pair of infrared light emitting diodes (LEDs) (900 nm peak; 100 nm FWHM) on each side of the aperture. The LEDs have a finite size so they subtend an eccentricity from 0 to 3 mm. The side of the LED facing the aperture was filed off to allow for minimum eccentricity and to provide a straight edge for the limiting aperture. A schematic of the LED and aperture is shown on the inset of Fig. 1. The eccentric photorefractor assembly was fitted onto a standard CCD camera lens. Infrared illumination was used because of high LED radiant power, high retinal reflectivity and most importantly because the infrared illumination does not distract or provide an accommodative stimulus for the subject. Under dim conditions, the LEDs were only faintly visible because the spectrum of the LED extended into the visible range.

The small aperture maximized the ratio between refracted and scattered light returning to the camera. Scattered light was minimally detected by the small aperture (since the scattered light that is detected varies with the area of the camera aperture) but the aperture did not reduce the refracted light, which travels in a narrow beam after being reflected and refracted from
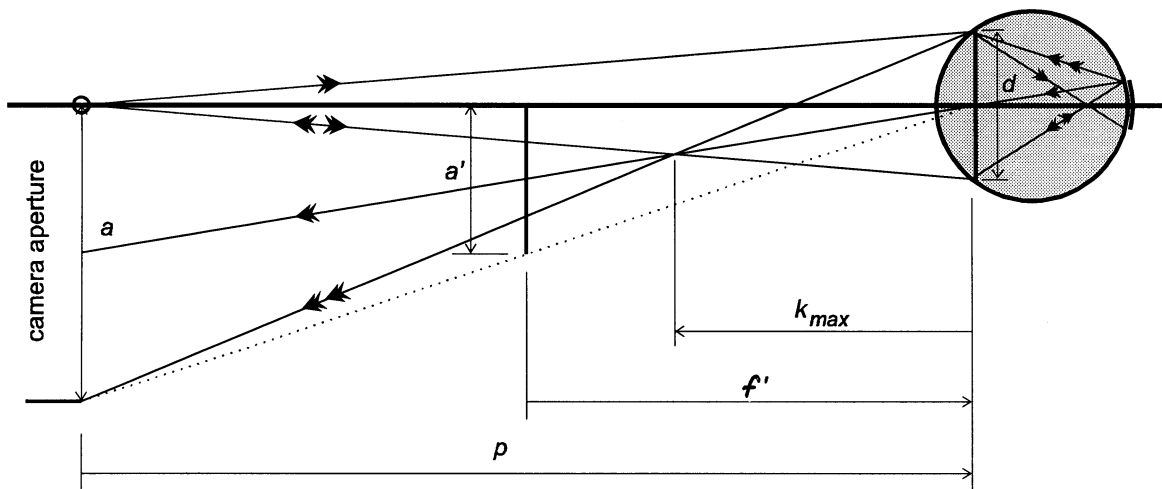
Fig. 2. This ray diagram is used to define the maximum amount of defocus k_{max} from the apparent camera position allowed before vignetting occurs. The apparent size of the camera aperture is defined by the fact that the aperture subtends the constant angle at the eye irrespective of its distance behind the optometer lens. The dotted line is a construction used to define the edge of the apparent camera aperture. The first ray to be vignetted by the opposite side of the camera emerges from the extreme edge of the retinal blur. The retinal blur is illustrated as the solid line just posterior to the eye on the figure. The ray diagram shows the condition where a ray from the edge of the blur just strikes the opposite camera aperture (double arrow). For myopia greater than the amount shown, this ray will miss the camera aperture and be vignetted. To determine the amount of defocus at which vignetting occurs, some fundamental relationships have to be derived. The apparent aperture size, a, is related to the apparent distance of the image of the photorefractor viewed through the Badal lens, p, by:

$$\frac{a}{p} = \frac{a'}{p'} \Rightarrow p = \frac{f'a}{a'}$$

where a' is the actual size of the photorefractor aperture and f' is the distance from the optometer lens to the eye. The distance k_{max} is the most myopic far point for which there is no vignetting. The distance k_{max} is derived from similar triangles such that

$$\frac{d}{-k_{max}} = \frac{a}{p + k_{max}} \Rightarrow \frac{1}{-k_{max}} = \frac{1}{p}\left(\frac{a}{d} + 1\right)$$

The amount of defocus from the apparent photorefractor position (in dioptres) is given by:

$$\Delta D = \frac{1}{-k_{max}} - \frac{1}{p} = \frac{1}{p}\left(\frac{a}{d} + 1\right) - \frac{1}{p} = \frac{1}{p}\left(\frac{a}{d}\right) = \frac{a'}{f'd}$$

The result shows that there is simple relationship defining the maximum amount of defocus for which no vignetting occurs. This result is independent of the photorefractor distance. For example, if the pupil size is 8 mm, the photorefractor aperture is 8 mm and the optometer lens is 250 mm, then the defocus from the camera position would have to be 4 D before vignetting. For smaller pupil sizes, the amount of defocus would have to be greater. This result demonstrates that with our system vignetting is not a problem for small refractive errors.

the eye. Vignetting of the refracted rays by the opposite side of the camera aperture only arises in the case of large amounts of defocus. For example, if the eye has a pupil diameter of 8 mm and the optometer lens focal length is 25 cm, then refracted light from defocus errors less than ± 4 D from the camera position will not be blocked by the opposing edge of the camera aperture. This relationship is derived in the caption for Fig. 2.

Each pair of LEDs is run independently. Horizontal and vertical LEDs measure aberration and defocus changes in the horizontal and vertical meridia, respectively. Two orthogonal measurements are not sufficient in practice to measure astigmatism because of the potential for ambiguous results. Even measurements taken along three meridians have not been very reliable [15,16]. In order to obtain a complete refractive state measurement, the instrument could be built with more

LEDs around the aperture or the aperture and LED assembly could rotated about the camera axis. The LEDs are run by a 5 V, 0.5 A power supply and a control box. The control box is a constant-voltage/adjustable-current supply that allows switching of individual pairs of LEDs and provides a fine control so that the radiant power of each pair can be equalized.

2.2. Badal optometer

The eccentric photorefractor is moved behind a Badal optometer lens (Fig. 1) until its position is conjugate with the retina (positioned at the far point of the eye). The optometer lens is set a distance equal to its focal length from the eye. The use of a Badal optometer provides four advantages in that the power scale changes linearly with camera position and the sensitiv-

ity, irradiance at the eye and focal setting of the camera all remain unchanged with camera position.

2.2.1. Linear power scale

The apparent distance of the photorefractor is determined by its position behind the optometer lens according to the standard Badal formula,

$$L = F_{\text{lens}} \times \left(1 + \frac{l_{\text{opt}}}{f'_{\text{lens}}}\right) \tag{1}$$

where L is the apparent vergence of light from the photorefractor, l_{opt} is the distance from the optometer lens to the photorefractor, f'_{lens} is the secondary focal distance of the optometer lens, and F_{lens} is the power of the optometer lens in dioptres. With the Badal optometer design, the apparent position of the photorefractor in dioptres is linearly related to actual distances of the photorefractor behind the optometer lens [17].

2.2.2. Uniform sensitivity

The sensitivity of an eccentric photorefractor refers to its ability to detect changes in defocus for far points near the photorefractor position. Based on the basic optics of crescent formation [8], the sensitivity can be defined as the reciprocal of the angle subtended at the subject between the light source and the aperture edge or,

$$\text{sensitivity} = \frac{1}{\alpha} \approx \frac{d}{e} \tag{2}$$

where α is the subtended angle which can be approximated for small angles by the ratio of the eccentricity of the source, e, over the camera-to-subject distance, d. One of the fundamental properties of a Badal optometer is the fact that an object subtends a constant angle at the eye with changing distance behind the optometer lens [17]. Therefore, when the photorefractor is moved behind the optometer lens, the apparent size of the photorefractor is unchanged and thus the sensitivity remains constant at all distances. This would not be the case if a photorefractor were moved without the Badal optometer.

2.2.3. Constant irradiance at the eye

The irradiance of the LED source at the eye is constant for any distance of the eccentric photorefractor behind the optometer lens. This is shown theoretically below and has been verified in the laboratory. Without the optometer lens, the irradiance at the eye would vary inversely with the square of the distance of the photorefractor from the subject.

The irradiance of a point light source from the photorefractor measured at the optometer lens decreases by the square of its distance from the lens to give

$$H\text{lens} = \frac{P}{4\pi l^2} \tag{3}$$

where H_{lens} is the irradiance at the lens, P is the power of the light source and l is the distance from the optometer to the lens.

After refraction by the optometer lens, the light from the source is in a converging or diverging cone where the flux is constant but the irradiance changes with the area of the waist of the beam. The ratio of the irradiance at the eye to the irradiance at the lens is equal to the ratio of the area of the beam waist at the lens to the area of the beam waist at the eye (Fig. 3). The eye is at the focal point of the optometer lens and the light from the photorefractor source converges to or diverges from its image at a distance l' from the optometer lens (calculated with the thin lens equation).

The ratio of the areas of the beam waist at the optometer lens and at the eye can be calculated geometrically and is shown in Fig. 3. The ratio is the square of the radius of the beam at each position which by similar triangles is equal to the ratio of the squares of the cone heights.

$$\frac{H_{\text{eye}}}{H_{\text{lens}}} = \frac{4\pi r^2_{\text{lens}}}{4\pi r^2_{\text{eye}}} = \frac{r^2_{\text{lens}}}{r^2_{\text{eye}}} = \frac{l'^2}{(l'-f')^2} \tag{4}$$

The irradiance at the eye is given by the irradiance at the optometer lens multiplied by the above ratio where the relationship between l' and l is given by the thin lens formula.

$$H_{\text{eye}} = \frac{P}{4\pi l^2} \times \frac{l'^2}{(l'-f')^2} = \frac{P}{4\pi l^2} \times \frac{\left(\dfrac{l}{1+\dfrac{l}{f'}}\right)^2}{\left(\left(\dfrac{l}{1+\dfrac{l}{f'}}\right)-f'\right)^2} = \frac{P}{4\pi f'^2} \tag{5}$$

The irradiance at the eye depends directly on the power of the light source P and inversely on the square of the focal length of the Badal lens. The position of the photorefractor behind the Badal lens does not affect the irradiance of the light source at the eye. The actual light source extends over 3 mm but the same argument applies since the extended source can be considered as a superposition of independent point light sources. The radiance conservation theorem [18] states that the radiance of the photo-optometer light source at the eye will also be conserved. The conservation of radiance also follows from the fact that both the irradiance and the magnification of the source are unchanged with the light source position behind the optometer lens.
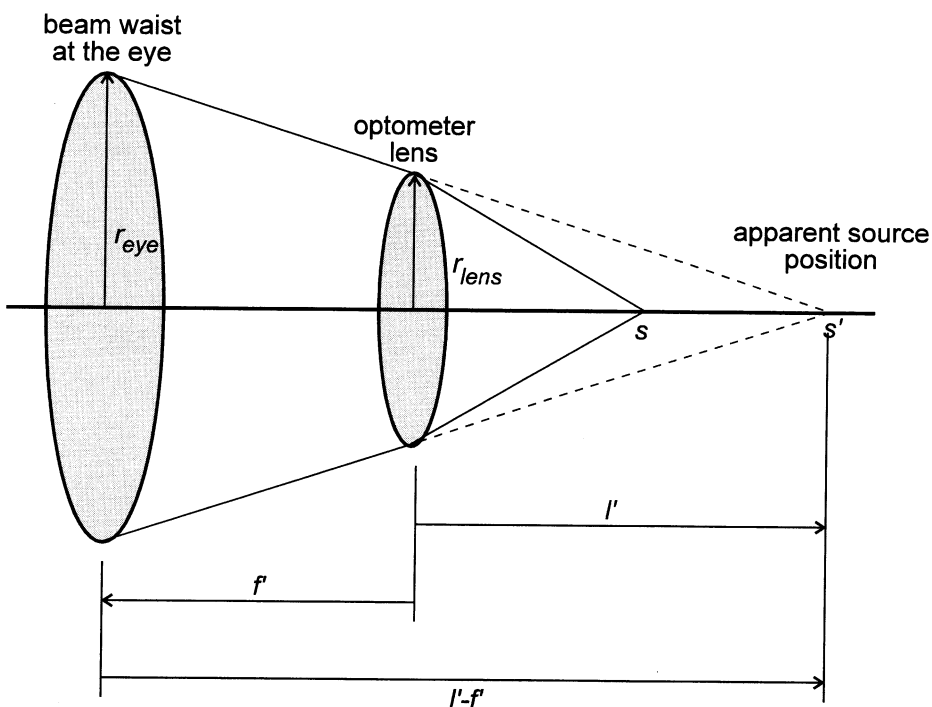
Fig. 3. The figure shows a divergent pencil of light emerging from an apparent source position s′ that is behind the optometer lens. Using similar triangles, it can be seen that the ratio of the areas of the shaded circles is equal to the ratio of the squares of the heights of the cones l' and $l' - f'$.

2.2.4. Constant focus

The camera of the photorefractor focuses on the subject's pupil. Since the subject is at the primary focal plane of the optometer lens, the apparent position of the subject will be at optical infinity for all positions of the photorefractor. Thus, the camera focus can remain fixed as the camera moves.

2.3. Hardware

A figure of the basic instrument is shown in Fig. 1. The optometer lens was a 4 D meniscus lens with a diameter of about 3.5 cm. The meniscus lens was used to minimize the reflected light entering the camera aperture.

A cold mirror was placed in the path to allow the presentation of visible fixation targets for the subject. The cold mirror (Melles Griot) was specifically designed for use at 45°. It provides a transmission of 85% (800–2500 nm) for infrared light and a reflection of 95% (400–700 nm) for 632 nm light and for most of the visible spectrum.

An optional artificial pupil could be placed immediately in front of the subject's eye and aligned with the axis of the instrument. The subject could rest in a chin rest or a bite bar. The chin rest or bite bar could be moved in the $x-y-z$ directions to allow for proper alignment of the subject behind the artificial pupil.

The eccentric photorefractor and camera assembly were mounted on a sliding track to allow them to move freely along the axis behind the optometer lens. A scale mounted along the track was used to record the camera position. The specific camera used in the instrument was a Canon Ci-20PR infrared-sensitive CCD camera. The automatic gain setting was turned off so the operator could have full control over the gain and offset of the signal. A Nikon 50 mm camera lens was connected to the CCD with an F-C mount adapter.

The computer was a 486 PC running at 50 MHz. It was equipped with a Coreco Oculus 300 frame grabbing card. Video output from the camera went directly to the frame grabbing card and subsequently to a monochrome video monitor for continuous viewing of the pupil image.

2.4. Software

Images from the frame grabbing board were read into the computer using a custom program written in Borland C + +. The ODX interface library of commands (Coreco, Canada) was used to communicate with the frame grabbing board.

The program read image buffers from the frame grabbing board for analysis. The speed of the program was optimized by reading images from a 150×200 pixel array in the centre of the 512×512 video image. A box showing the active window was displayed on the video monitor so that the subject's pupil could be easily aligned. Pupil images had to be within this window.

2.4.1. Image enhancement

Images were optimized by providing active control of the gain and offset of the CCD signal. These parameters were used to scale the signal before digitization so that the information obtained could be maximized. Adjustment was generally made until the range of gray levels in the image spanned the 8-bit pixel range. In the applications where the nulling procedure was used, the gain and offset of the signal could be adjusted freely without changing the fundamental performance of the instrument.

2.4.2. Finding the pupil edges

The pupil edges were found by a simple thresholding technique. Individual pixel values were read outwards from the centre of the array until the pixel value was below a specified threshold value. This point denoted the pupil edge. The top, bottom, left and right pupil edges were found in this manner line by line across the image. The computer looked for the width and position of the maximum pupil diameter in both the horizontal and vertical meridians. Crosshairs locating the positions of the pupil edges and the position of maximum diameter were displayed on the monitor so that the operator could ensure that the computer was tracking the pupil properly.

2.4.3. Intensity profiles

The gray scale image intensity profiles along the maximum horizontal and vertical pupil diameters were plotted on the screen. All the information about the refractive state of the eye was deduced from the changes in these intensity profiles. In order to use the instrument as an optometer, the slope of the intensity profile had to be calculated. A routine in the C + + program was used to calculate a least squares best-fit slope estimation for the maximum vertical and horizontal meridians. The value of the slope was continually plotted to a graph on the computer monitor to show continuous changes in profile slope over time.

2.5. Eccentric photo-optometer operation

In a separate paper [19], changes in reflex slope caused by changes in the ocular defocus state were modeled. It was shown that when an aberration-free eye was focused on the photorefractor, the intensity profile was flat. For an eye with aberrations, the profile was flattest when the eye was in the best focal state for viewing the photorefractor (given by the minimum rms wavefront error). The model showed that outside of this position, the slope of the profile became more positive or negative depending on the direction of defocus. In the eccentric photo-optometer, the refractive state of the eye remains constant while the photorefractor is moved in and out of the focal plane of the eye. With a 4 D optometer lens, the camera can move through a range of far point positions from hyperopia through to 4 D myopia. The static accommodative state is found by manually moving the photorefractor into a position where the slope of the reflex is zero. At this position, the photorefractor is coincident with the far point of the eye. Since infrared light is used, the far point positions have to be corrected for the extra hyperopia due to chromatic aberration of the 900 nm light (see section 4.1).

In actual experiments, both accommodation and camera movements caused changes in the profile slope. Accommodative changes in the eye could be monitored by following the changing slope of the reflex over time while the camera was stationary. This is analogous to the dynamic measurements of Schaeffel et al. [9]. The potential application of this instrument to dynamically measure accommodation is discussed in section 5.3.

3. Theoretical model

Using the technique described by Roorda et al. [19], the expected changes in reflex slope that would occur in this particular instrument have been modeled. The photorefractor was modeled with a similar light source to the actual optometer (extending from 0 to 3 mm eccentricity). The results of the simulation for four conditions, including no aberration, spherical aberration, coma and aberrations for a typical human eye are shown in Fig. 4. The aberrations for the human eye were measured across the horizontal meridian of the left eye of subject AR using a psychophysical technique [20]. In the simulation, the abscissa was plotted as camera position which varied linearly with refractive state. With a 4 D optometer lens, each change in camera position of 62.5 mm corresponds to 1 D of defocus. The figure shows that the eccentric photo-optometer detects continuous changes in intensity profile slope with camera position for all the modeled conditions. The plots are also very linear showing an almost constant rate of change in slope with camera position. The reason for this is because the source is extended from zero eccentricity (to increase sensitivity and minimize the dead zone) out to a relatively large eccentricity given the short working distances used (to increase the working range) [19]. Although the directionality of the reflection has been incorporated into the model in a previous paper [13], it was not incorporated into this model because of the infrared light source. It is expected, since infrared light penetrates deeper into the fundus [21], that the reflection is less directional than that for shorter wavelengths.

In subsection 2.2.2, the sensitivity of the photorefrac-

(a) no aberration

(b) spherical aberration
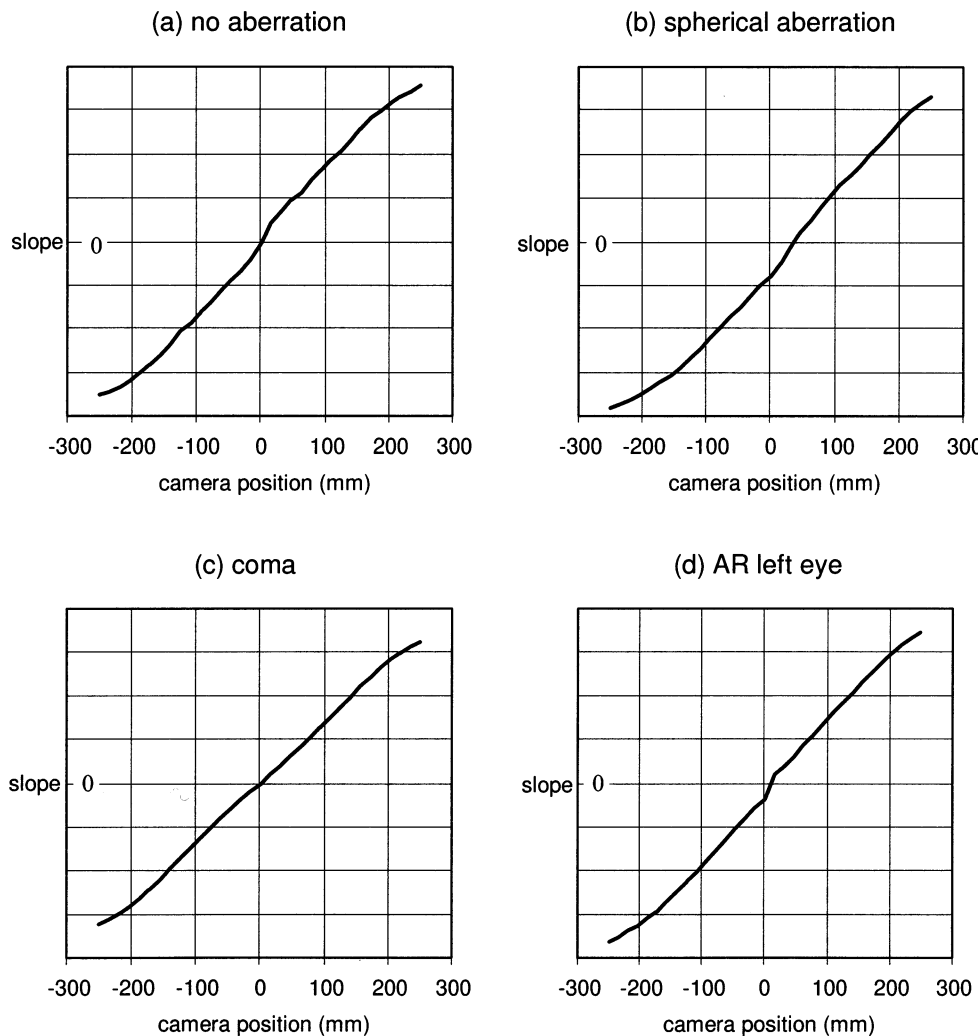
(c) coma

(d) AR left eye

Fig. 4. The plots represent the expected changes in the slope of the photorefractive reflex as the camera is moved. For the 4 D optometer lens, 1 D of defocus corresponds to 62.5 mm of camera movement. The camera motion of ± 250 mm, therefore spans a dioptric defocus range of ± 4 D. The simulations are for an extended source spanning a range from 0 to 3 mm in eccentricity. All conditions are the same between plots except that the aberrations are different. The amounts of third order spherical aberration and coma were set such that they each produced 0.93 D aberration at the edge of the 5 mm pupil. The aberrations for subject AR were for the left eye along the horizontal meridian under normal conditions while viewing a target at 2 m. The best-fit slopes for all curves were all within 2% of each other except the slope of the curve for coma which was less by 13%. The plot for spherical aberration is shifted horizontally toward hyperopia. The amount of shift with respect to the 0 mm camera position is 40 mm, corresponding to 0.64 D. This shift, however, corresponds quite closely to the best defocus position for an eye with such aberrations (based on the amount of defocus required to minimize the root mean square aberration).

tor was defined as the ratio of the working distance over the eccentricity. In theory, this eccentric photorefractor has infinite sensitivity since the eccentricity goes to the edge of the camera aperture. The infinite sensitivity implies that there is no dead zone and there are continuous changes in slope of the intensity profile with changing camera position or refractive state. This is seen in the modeled results on Fig. 4. In practice, the sensitivity is limited by other factors such as scatter in the optical system of the eye, accommodative fluctuations, tear film and the light sensitivity of the camera system. The performance of the instrument, therefore, is better defined empirically by measuring the repeatability (see section 4.2).

4. Empirical testing and accommodative stimulus/response experiments

4.1. Correction for the infrared light source

The refractive state estimations made using infrared light were more hyperopic than would be expected from visible light measures because of chromatic aberration in the eye and differences in the retinal reflecting surface as a function of changing wavelength [22,21]. The amount of this difference was determined empirically. The eye of one near-emmetropic subject with normal vision was cyclopleged with two drops of 1% cyclopentolate and refractive state was measured by retinoscopy.

A Wratten 29 gelatine filter was placed in front of the eye of the retinoscopist so that the refraction was referenced to 632 nm. The retinoscopy was performed while the subject was in the apparatus viewing through the 5 mm pupil of the photo-optometer. This served to minimize differences between techniques because of monochromatic aberrations. The refraction of the subject was then measured through the same pupil with the eccentric photo-optometer. The subject was kept stationary in a bite bar. After each neutralization of the slope (see subsection 2.4), the subject sat out of the instrument, the position of the camera was recorded and the camera was moved out of position.

Ten photorefractive measures for the single cyclopleged subject yielded an estimation of refractive state of 0.53 D with a standard deviation (S.D.) of 0.048 D. The actual refractive state of the eye at 632 nm measured by retinoscopy was 0.076 D (to within 0.12 D accuracy). The correction factor was taken as the difference between these two values, i.e. 0.44 D. Each refractive state measured by the instrument was corrected by this amount to yield a refractive state referenced to 632 nm. These values can be further corrected to give refraction for any wavelength. For example, a correction to 555 nm would require an additional correction of about 0.35 D based on a summary of well-established values of the chromatic aberration for the human eye [17]. This value is similar to corrections used by other infrared optometers with similar spectral characteristics [17].

4.2. Repeatability and precision

The data acquired for the correction of the chromatic aberration of the infrared light source were also used to calculate the repeatability of the instrument. Ten neutralization measurements were made. The range of camera positions was from 278 to 287 mm with a standard deviation of 2.98 mm corresponding to a dioptric range of 0.14 D, with S.D. = 0.048 D.

4.3. Measurement of stimulus-response functions of accommodation

To test the instrument, the accommodation in response to a changing stimulus was measured for a 5 mm pupil size and repeated with a 0.5 mm pinhole before the fixating eye [23]. The nature of the accommodative responses to these two conditions are well known. In the former case, the typical lead-lag function of accommodation is expected [24–26]. In the latter case, a 'flat' accommodative response is expected [23].

The subjects were aligned in a chin rest or bite bar mount such that the eye was at the primary focal point of the optometer lens. The subject was given a fixation target to view through a cold mirror beamsplitter placed in the optical path between the eye and the optometer lens. The camera imaged the subject's pupil through a 5 mm artificial pupil placed immediately in front of the subject's eye. The subjects were instructed to maintain fixation on the target. The room lights were dimmed for all experiments.

The gain and offset of the signal from the CCD camera were adjusted for each subject in order to provide sufficient signal for analysis. While the subject maintained fixation, the photorefractor was moved along the sliding track behind the optometer lens while the slope of the light intensity distribution across the pupil was continually recorded on the computer monitor. The experimenter moved the photorefractor until the slope along the vertical meridian was estimated to be zero.

In the first experiment, the subject used normal fixation on a high contrast target through a 5 mm artificial pupil. The target was a 1 cm Snellen E. The fixation target was illuminated using a conventional incandescent lamp.

In the second experiment, the subject fixated on the same target but this time through a 0.5 mm pinhole. The 0.5 mm pinhole was drilled into an infrared transmitting filter (Kodak Wratten 89b). The infrared photorefractor light was unaffected by the filter and thus the entire pupil could be measured. The subject, however, could only see the visible target through the 0.5 mm pinhole.

The high contrast target was placed at 1.8 m from the eye (0.56 D stimulus). The stimulus to accommodation was varied by placing trial lenses of increasing negative power in front of the eye. A stimulus range from 0.56 to 5.56 D was presented in 1 D steps. All lenses were randomly selected until three trials had been completed for each stimulus level. During the experiment, neither the experimenter nor the subject were aware of the power of the lens introduced. The negative lens diverged the light returning to the photorefractor from the accommodated eye. The null position of the photorefractor was remotely displaced by a magnitude corresponding to the dioptric power of the lens. This distal displacement of the photorefractor provided two advantages. Firstly, the accommodative responses which could be measured were no longer limited to less than 4D by the physical presence of the Badal lens. Instead accommodative responses to any stimulus level could be measured as long as the accommodative response did not exceed the stimulus by more than 4D. Secondly, the intensity of the reflections from the Badal lens were reduced.

4.4. Results of stimulus/response measurement of accommodation

Stimulus/response data for the three subjects are

shown in Fig. 5 (a, b, c). The best-fit line for each set of data is shown on the graphs. The data points represented individual measurements of the accommodative response of the subjects.

As expected, the subjects' accommodative responses through the 0.5 mm pinhole were considerably flatter than when viewing through the whole pupil. Based on
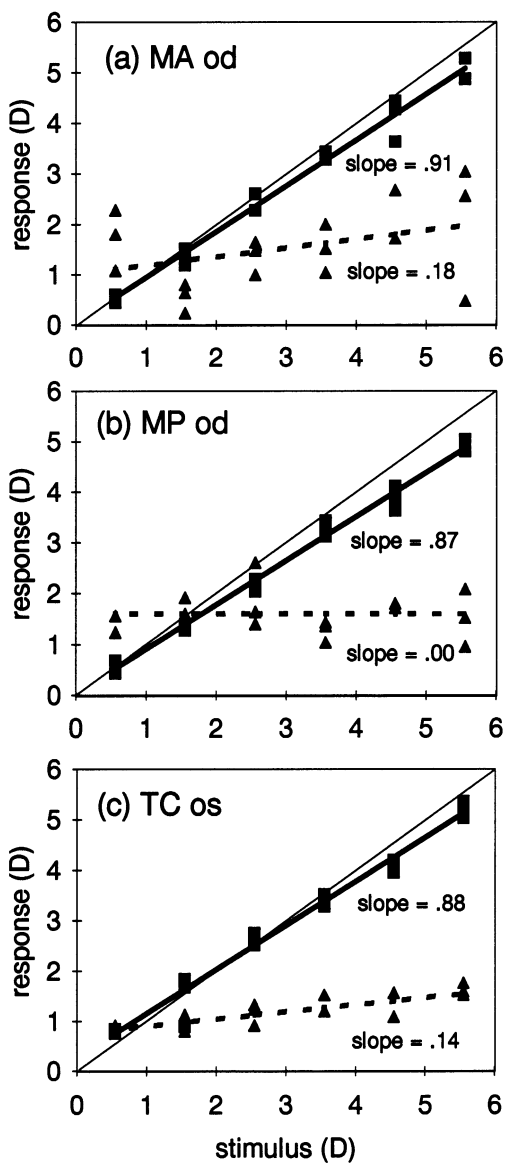

Fig. 5. Accommodative stimulus/response plots for three subjects. The square symbols are data points for subjects viewing the high contrast target through large pupils. The best fit slope is the solid line. The triangle symbols are data points for viewing through the 0.5 mm pinhole. The best fit slope is the dashed line. The slopes for the best fit lines are just below the lines on each plot. The thin solid line is the ideal response line, or 1:1 line. Based on 95% confidence intervals, the slopes for the 0.5 mm pinhole response/stimulus curves were not significantly different from zero for subjects MA and MP. (a) Subject MA was a 1.5 D myope, aged 29, wearing soft contact lenses and used a bite bar. (b) Subject MP was an emmetrope with no correction, aged 28 and used a bite bar. (c) Subject TC was a 4.5 D myope with a soft contact lens correction, aged 26 and used a chin rest.

95% confidence intervals in the regression analysis, the slopes for subjects MA and MP for the pinhole case were not significantly different from zero. The slope for TC was significantly different from zero but was very small (0.14). For the high contrast target viewed through a 5 mm pupil, the response was very close to the stimulus. As expected, the slopes were less than one, illustrating the well-established lead and lag of accommodation typical of such functions [24–26]. The variability of the accommodative response was less for the 5 mm pupils versus the 0.5 mm pinhole. These results compare favorably with similar experiments that measured accommodation with the Canon AutoRef R-1 [23]. The small, but significant, difference in the slope from zero for subject TC may indicate that, for some subjects, a 0.5 mm pinhole does not fully open the loop of accommodation.

The static accommodative response estimations varied from measurement to measurement, especially for the small pinhole. The greater fluctuation for the smaller pupil was expected since the depth of focus was increased to allow a greater range of accommodative state for which the target remained subjectively in focus. Variations in accommodative state were also observed for the larger pupil sizes but these were small. The largest range of static accommodative response for a single stimulus with a high contrast target and the 5 mm pupil was 0.64 D for subject MA with the 4.56 D stimulus. These variations in accommodative state are similar in magnitude to those observed by other authors [23] and are in agreement with measurements of the depth of focus of the human eye for changing pupil sizes [27].

5. Discussion

5.1. Performance of the eccentric photo-optometer

The instrument presented in this paper has been used to measure successfully the accommodative response to a stimulus for three different conditions. The instrument performance was as predicted from the theoretical analysis. The theoretical model demonstrated that, with the particular eccentric photorefractor light source configuration, the ability to detect changes in slope near the neutralization position would not vary greatly between individuals with different aberrations. These continuous changes in slope with camera position were also observed in the experiment, confirming that the instrument had no observable dead zone. The instrument makes highly repeatable measurements of refractive state (S.D. = 0.048 D) when an eye is cyclopleged.

In the stimulus-response experiments, the main difficulties were in measuring static accommodation

when, in fact, the accommodative state of the subject was continually fluctuating. The accommodative fluctuations, however, could be tracked by monitoring the changing intensity profile slope while the camera remained stationary. The slopes were neutralized during periods when the accommodation was relatively stable and, by performing three measurements for each stimulus, a representative range of the accommodative fluctuations was shown. With a dynamic measure of accommodation, these fluctuations could be measured directly (see subsection 5.3).

Refractive state estimations were made along the vertical meridian only. None of the subjects in this study had any significant amount of astigmatism. In order to perform an accurate measure of the refractive state, the photorefractor assembly could be rotated to measure refraction along multiple meridia.

5.2. Control of aberrations.

Aberrations in the eye are known to affect the intensity profiles in eccentric photorefraction. When the eye has aberrations, intensity profiles no longer follow a smooth slope. Split profiles and sharp intensity variations are all possible depending on the specific aberration [13]. True neutralization of the reflex is often not possible. However, modeling of the configuration of this photorefractor (Fig. 4) shows that the best fit slope varies continuously and monotonically with changes in camera position so a neutral position can always be found. When aberrations are present, the camera position for the neutral slope may be shifted slightly due to the change in the average power of the eye [19]. The rate of change of slope with camera position, however, changes very little when aberrations are present so the sensitivity of the instrument is not affected greatly. As the pupil size decreases, aberrations reduce, the slope becomes more linear and the flattest slope corresponds most closely with the paraxial refractive state [19].

In the experiments, a 5 mm artificial pupil was used, situated coaxial with the photorefractor. The 5 mm pupil was used to avoid using the periphery of the optical system where the aberrations are generally the highest [28,20] and to maintain a constant pupil size between subjects. The subject was kept stable in a bite bar or chin rest and allowed to see the fixation target through the artificial pupil. The subject was moved up, down and sideways behind the artificial pupil until relatively linear intensity profile variations were observed. The intensity profiles were usually most linear when the artificial pupil was centered over the actual pupil. Two other methods to control the pupil size are to project an artificial pupil onto the subject's eye or to stimulate natural pupil constriction with ambient light conditions.

5.3. Considerations for dynamic accommodation measurements

In this paper, static measures of accommodation were recorded by nulling the slope of the reflex. However, in order to measure dynamic accommodation, movement of the camera would not be practical. Therefore, to make a dynamic measurement the refractive state would have to be inferred from the slope of the reflex. In order to do this, the exact relationship between changes in profile slope with refractive error needs to be established. This calibration is best achieved by empirical measures. The common calibration method has been to place a sequence of trial lenses in front of an eye to simulate refractive state changes while recording the corresponding changes in slope. The eccentric photo-optometer, however, can be calibrated using a faster technique. The calibration of the eccentric photo-optometer is based on the fact that slope of the reflex induced by having the far point of the eye moved away from the camera plane by 1 D is equivalent to the slope induced by moving the camera position out of the far point plane by 1 D. Using this fact, the calibration can be achieved by recording the slope while the camera is moved to known dioptric distances from the far point of an eye whose accommodative state is fixed. This set of slope values could then be converted into a function or look-up table that defines the slope as a function of accommodative state. The recording of the calibration values could be easily automated so that fast, unique and accurate calibrations could be performed for any subject under any operating conditions. In this way, a calibration could be derived for the specific eye being measured after the gain and offset had been set to maximize the signal, which would depend on individual pupil sizes and aberrations. For larger pupil sizes, averaging responses for sources either side of the aperture would reduce changes in calibration with pupil size due to asymmetric aberrations [19,16]. In the actual dynamic operation, the camera would remain stationary while the computer measured the slope and calculated the changes in the subject's accommodative state over time.

5.4. Comparison with conventional eccentric photorefraction

The modern eccentric photoretinoscope estimates the refractive error of the eye based on a measurement of the slope of the photorefraction profile [9]. This is reliable provided that a proper calibration of the instrument has been made and that the eye is free of aberrations. The slope-based photorefractor is an ideal screening instrument given its speed and ease of operation. The main difficulty, however, is in the calibration and the corresponding need to operate under similar

lighting conditions at all times. The modeling of slope-based eccentric photorefractors [19] showed that instrument calibration is dependent on the monochromatic aberrations of the eye and changes in pupil size.

To avoid the need to calibrate, photorefraction techniques can neutralize the pupillary light reflex by placing trial lenses in front of the eye being measured [14,29]. Neutralizing the reflex in this manner is not possible for accommodation experiments since the optical vergence of the stimulus changes with the power of the lens placed in front of the eye. The photo-optometer has the advantage of neutralizing the slope without the use of a trial lens.

5.5. Comparison with other objective optometers

There are no other objective optometers that have combined eccentric photorefraction principles with the Badal optometer. The commercially available Humphrey Automatic Refractor model 505 (Humphrey Instruments, San Leandro, CA) has some similarities in that it uses a knife edge aperture, an eccentric source and infrared illumination with a Badal optometer [17]. However, the instrument does not determine the slope of the reflex. Instead, it images the pupil and the crescent reflex onto a split photo-detector. Refractive error is determined by an optical adjustment that equalizes the intensity of the reflex from either side of the pupil. This technique is analogous to neutralizing the slope except that it balances the signal from only two detectors. Furthermore, it is not video-based and does not allow remote fixation targets or have the potential to provide dynamic measures. Other instruments to objectively measure accommodation are based on differing optical principles that include: Scheiner's disc principle [30,4,31,32]; double pass image quality [33,34]; Purkinje images [35]; and, streak retinoscopy [36,5]. No quantitative comparison has been made of the performance of this device compared to others.

The advantage of this design over other designs for measuring refractive state is that it can be made relatively insensitive to ocular aberrations and to eye misalignments and head motion. Aberrations of the eye are a concern for all refraction methods and it is impossible to use a general correction since aberrations vary from individual to individual [37,28,20]. This instrument is much less sensitive to aberrations than photorefractors which measure crescent extent. Being robust with respect to eye misalignments and head motion make it a good candidate for studies with untrained subjects. The current design analyzed only a small portion of the entire video image from the CCD camera. This was done to optimize the speed of the analysis. With more sophisticated hardware, the frame size could be enlarged allowing more eye movement and measurement of two eyes simultaneously. If these changes were made,

the instrument would have broad applications to clinic patients, including accurate measurements of accommodation in children. Given that the instrument images both the pupil and the corneal reflex, binocular measurements of the near triad response could be possible. The video feedback to the experimenter allows monitoring of other factors such as tear film break-up, contact lens misalignment or squinting.

6. Conclusions

The eccentric photo-optometer is a convenient method for measuring refractive state and accommodation in the human eye.

Static accommodative measures can be performed quickly and accurately without the need to calibrate the instrument. The instrument has adjustable gain and offset allowing measurement under many different lighting conditions. The use of the cold-mirror allows the introduction of any type of accommodative stimulus.

The eccentric photo-optometer can also be adapted to measure other ocular properties. These include dynamic accommodation, using a simple procedure to quickly calibrate the instrument for any change in lighting or experimental conditions. With suitable hardware and software modifications, the instrument can also measure two eyes simultaneously and measure the near triad response.

References

[1] Alpern M, Ellen PA. A quantitative analysis of the horizontal movements of the eyes in the experiment of Johannes Mueller: I. Methods and results. Am J Ophthalmol 1956;42:289–303.

[2] Knoll HA. Measuring ametropia with a gas laser. Am J Optom Arch Am Acad Optom 1966;43:415–8.

[3] Charman WN. On the position of the plane of stationarity in laser refraction. Am J Optom Physiol Opt 1975;51:832–8.

[4] Campbell FW, Robson JG. High speed infrared optometer. J Opt Soc Am 1959;49:268–72.

[5] Kruger PB. Infrared recording retinoscope for monitoring accommodation. Am J Optom Physiol Opt 1979;56:116–23.

[6] McBrien NA, Millodot M. Clinical evaluation of the Canon Autoref R-1. Am J Optom Physiol Opt 1985;62:786–92.

[7] Rosengren B. A method of skiascopy with the electric ophthalmoscope. Acta Ophthalmologica 1937;15:501–11.

[8] Bobier WR, Braddick OJ. Eccentric photorefraction: Optical analysis and empirical measures. Am J Optom Physiol Opt 1985;62:614–20.

[9] Schaeffel F, Wilhelm H, Zrenner E. Inter-individual variability in the dynamics of natural accommodation in humans: Relation to age and refractive errors. J Physiol 1993;461:301–20.

[10] Howland HC. Optics of photoretinoscopy: Results from ray tracing. Am J Optom Physiol Opt 1985;62:621–5.

[11] Bobier WR. Eccentric photorefraction: A method to measure accommodation of highly hypermetropic infants. Clin Vision Sci 1990;5:45–66.

[12] Uozato H, Saishin M, Guyton DL. Refractive assessment of infants with infra-red video-refractor PR-1000. Invest Ophthalmol. Vis Sci 1991;4:12–38.

[13] Roorda A, Campbell MCW, Bobier WR. Geometrical theory to predict eccentric photorefraction intensity profiles in the human eye. J Opt Soc Am A 1995;12:1647–56.

[14] Schaeffel F, Farkas L, Howland HC. Infrared photoretinoscope. Appl Opt 1987;26:1505–9.

[15] Phillips D, Sterling W, Dwyer WO. Validity of the laser refraction technique for determining cylindrical error. Am J Optom Physiol Optics 1975;52:328–31.

[16] Gekeler F, Schaeffel F, Howland HC, Wattam-Bell J. Measurement of astigmatism by automated infrared photoretinoscopy. Optom Vis Sci 1997;74:472–82.

[17] Bennett AG, Rabbetts RB. Clinical Visual Optics, 2nd edn. London: Butterworths, 1989.

[18] Zalewski EF. Radiometry and Photometry. In: Bass M, van Stryland EW, Williams DR, Wolfe WL, editors. Handbook of Optics, 2nd edn. New York: Mc-Graw Hill, 1995:24.3–24.51.

[19] Roorda A, Campbell MCW, Bobier WR. Slope-based eocentric photorefraction theoretical analysis of different light source configurations and effects of ocular aberrations. J Opt Soc Am A 1997;14:2547–56.

[20] Campbell MCW, Harrison EM, Simonet P. Psychophysical measurement of the blur on the retina due to optical aberrations of the eye. Vision Res 1990;30:1587–602.

[21] Delori FC, Pflibsen KP. Spectral reflectance of the human ocular fundus. Appl Opt 1989;28:1061–77.

[22] Charman WN. Reflection of plane-polarized light by the retina. Br J Physiol Opt 1980;34:34–49.

[23] Ward PA, Charman WN. On the use of small artificial pupils to open-loop the accommodation system. Ophthal Physiol Opt 1987;7:191–3.

[24] Fry G. An experimental analysis of the accommodation convergence relationship. Am J Opt 1937;14:402–14.

[25] Morgan MW. Accommodation and its relationship to convergence. Am J Opt 1944;21:183–95.

[26] Morgan MW. Accommodation and convergence. Am J Opt 1968;45:417–54.

[27] Charman WN. Optics of the human eye. In: Cronly-Dillon J, editor. Visual optics and instrumentation. Boca Raton: CRC Press, 1991:1–26.

[28] Walsh G, Charman WN, Howland HC. Objective technique for the determination of monochromatic aberrations of the human eye. J Opt Soc Am A 1984;1:987–92.

[29] Bobier WR, Schmitz P, Strong G, Knight J, Widdersheim K, Howland HC. Comparison of three photorefractive methods in a study of a developmentally handicapped population. Clin Vision Sci 1992;7:225–35.

[30] Collins G. The electronic refractionometer. Br J Physiol Opt 1937;11:30–42.

[31] Charman WN, Heron G. A simple infra-red optometer for accommodation studies. Br J Physiol Opt 1975;30:1–12.

[32] Lovasik JV. A simple continuously recording infrared optometer. Am J Optom Physiol Opt 1983;60:80–7.

[33] Pugh JR, Winn B. Modification of the Canon AutoRef R-1 for use as a continuously recording infra-red optometer. Ophthal Physiol Opt 1988;8:460–5.

[34] Munnerlyn CR. An optical system for an automatic eye refractor. Opt Eng 1978;17:627–30.

[35] Allen MJ. An objective high speed photographic technique for simultaneously recording changes in accommodation and vergence. Am J Opt 1949;26:279–89.

[36] Knoll HA, Mohrman R. The Ophthalmetron, principles and operation. Am J Opt 1972;49:122–8.

[37] Howland HC, Howland B. A subjective method for the measurement of monochromatic aberrations of the eye. J Opt Soc Am 1977;67:1508–18.